




## BaTiO<sub>3</sub>-assisted inorganic laser lift-off process for flexible micro-light-emitting diodes

**Han Eol Lee**, Division of Advanced Materials Engineering, Jeonbuk National University, Jeonju, Jeonbuk 54896, Republic of Korea; Department of JBNU-KIST Industry-Academia Convergence Research and Hydrogen & Fuel Cell Research Center, Jeonju, Jeonbuk 54896, Republic of Korea

**Chang Kyu Jeong** , Division of Advanced Materials Engineering, Jeonbuk National University, Jeonju, Jeonbuk 54896, Republic of Korea; Department of JBNU-KIST Industry-Academia Convergence Research and Hydrogen & Fuel Cell Research Center, Jeonju, Jeonbuk 54896, Republic of Korea; Department of Energy Storage/Conversion Engineering of Graduate School, Jeonbuk National University, Jeonju, Jeonbuk 54896, Republic of Korea

Address all correspondence to Han Eol Lee at [haneol@jbnu.ac.kr](mailto:haneol@jbnu.ac.kr) and Chang Kyu Jeong at [ckyu@jbnu.ac.kr](mailto:ckyu@jbnu.ac.kr)

(Received 5 April 2023; accepted 12 June 2023; published online: 29 June 2023)

### Abstract

Extensively studied transfer methods for producing high-performance flexible micro-light-emitting diodes ( $\mu$ LEDs) have limitations like high process cost and size constraints. Herein, we report a novel inorganic-based laser lift-off (ILLO) process, in which a new BaTiO<sub>3</sub> (BTO) sacrificial layer is used to fabricate flexible thin-film  $\mu$ LEDs. The process, associated laser conditions, and carrier substrate types were optimized using theoretical simulations and experiments. The BTO sacrificial layer was successfully applied to the ILLO process via laser–material interactions, as verified by material analyses. Vertically structured flexible  $\mu$ LEDs were realized using BTO-based delamination, demonstrating the method's applicability to next-generation electronics.

### Introduction

In the emerging Internet of Things (IoT) era, smart devices have been widely developed for information exchange in everyday life.<sup>[1–6]</sup> Flexible electronic devices have surfaced as next-generation replacements for currently commercialized smart devices.<sup>[7–9]</sup> In particular, flexible displays have been suggested as potential candidates for bilateral interaction via the exchange of visual information because they can be easily affixed onto a variety of surfaces, including human skin, garments, automobiles, and constructions.

Inorganic-based micro-light-emitting diodes ( $\mu$ LEDs), equipped with superior optical properties, minimal power consumption, short latency periods, prolonged lifespans, and high endurance in extreme environments, are considered desirable features in flexible displays.<sup>[10–12]</sup> Additionally, flexible  $\mu$ LEDs can be attached to dynamic surfaces to provide user-friendly optoelectronic devices based on human–machine interfaces (HMI) for virtual reality (VR), augmented reality (AR), and smart devices in hyperconnected cultures.<sup>[12–14]</sup> Various transfer approaches, including polydimethylsiloxane-based stamping, mechanical delamination, and electrostatic-force-induced chip transfer, have been proposed to obtain high-performance flexible  $\mu$ LEDs. However, the commercialization of  $\mu$ LED displays is difficult because of their high material and processing costs.<sup>[15,16]</sup> Moreover, to convert the  $\mu$ LED into various-sized displays depending on its intended application, the LED chip spacing must be freely modifiable; nevertheless, existing chip transfer methods cannot solve this problem.<sup>[10,11]</sup>

Recently, the inorganic-based laser lift-off (ILLO) process has been highlighted as a simple thin-film transfer technique

for resolving issues with existing transfer methods.<sup>[17–21]</sup> Electronic devices on an inorganic sacrificial layer are peeled off a mother wafer by laser–material interactions and transferred onto the target substrate. Although ILLO processes are adequate for achieving flexible thin-film electronics owing to their high transfer speed, large-scale processability, versatility, and selective transfer, they have intrinsic restrictions in that only specific materials can be utilized for sacrificial layers.<sup>[8,22,23]</sup> In addition, the existing III-N-based sacrificial materials (GaN, AlN, and InN) have to be dry etched under extremely harsh conditions (corrosive Cl<sub>2</sub> gas-based process) to remove residual materials, and PZT-based materials may have heavy metal substances of lead, causing environmental problems in post-processes.<sup>[17,18]</sup> Therefore, it is necessary to verify whether the ILLO process can be conducted using another material as a sacrificial layer without the aforementioned issues.

Herein, we report a new ILLO process using a BaTiO<sub>3</sub> (BTO) sacrificial layer for demonstrating vertically structured flexible  $\mu$ LEDs. The  $\mu$ LED chips, which were formed on a rigid GaAs wafer, were attached to a BTO-deposited transparent substrate and then exfoliated at the interface between the BTO and substrate by irradiation with a high-power-density UV laser. The heat distribution for the ILLO process was theoretically confirmed using finite element method (FEM) simulations. The laser conditions for ILLO were experimentally optimized to 750 mJ cm<sup>-2</sup> by analyzing the exfoliated surface using scanning electron microscopy (SEM) and X-ray diffraction (XRD) analysis. Finally, vertically structured flexible  $\mu$ LEDs were successfully fabricated on a polyethylene (PET) substrate via selective thin-film transfer using

the BTO-assisted ILLO process and device packaging using an anisotropic conductive film (ACF).

## Material and methods

### BTO thin-film deposition

BTO thin films were deposited onto transparent glass substrates using a radiofrequency (RF) sputtering equipment. Plasma from the BTO target was formed at a processing pressure of 6.5 mTorr, an Ar flux of 30 sccm, and an RF power of 118 W. The deposition was conducted for approximately 1 h to form a 300-nm-thick BTO thin film. Then, a plasma-enhanced chemical vapor deposition (PECVD)-generated silicon dioxide (PEO) thin film was deposited onto the BTO film as a buffer layer to distribute the laser-induced heat and mechanical stresses during the exfoliation stage.

### Laser irradiating system

An excimer laser (wavelength: 308 nm) was utilized to react with the BTO thin film to exfoliate the attached  $\mu$ LEDs. The pulsed laser shots were continuously scanned onto the BTO film at a frequency of 20 Hz, and the sample stage simultaneously moved in the  $x$ - and  $y$ -directions at a speed of 12 mm s<sup>-1</sup>. The laser shot used for material analyses (XRD and SEM) and  $\mu$ LED exfoliation had dimensions of 600  $\mu$ m  $\times$  600  $\mu$ m and 50  $\mu$ m  $\times$  55  $\mu$ m, respectively.

### Flexible $\mu$ LED fabrication

By using metal-organic chemical vapor deposition (MOCVD), AlInGaP LED layers were grown on a GaAs substrate by metal-organic chemical vapor deposition. The mesa structure of the  $\mu$ LED array (chip dimensions: 80  $\mu$ m  $\times$  80  $\mu$ m) was fabricated by inductively coupled plasma reactive-ion etching (ICP-RIE) with Cl<sub>2</sub> gas. After making p-ohmic contacts (Cr/Au) on the chip surface, the  $\mu$ LED array was attached to the PEO/BTO/glass substrate using an optical adhesive (Norland Optical Adhesive 61; NOA 61). The mother GaAs wafer was then etched by hydrogen peroxide (H<sub>2</sub>O<sub>2</sub>) and citric acid (C<sub>6</sub>H<sub>8</sub>O<sub>7</sub>) solution. After attaching the bottom side of the  $\mu$ LED array to the Au/PET substrate through an anisotropic conductive film (ACF), laser was focused at the interface between the BTO and glass and irradiated to delaminate the glass substrate. The stacked layers above the  $\mu$ LED array were removed using ICP-RIE with SF<sub>6</sub>/O<sub>2</sub>/Ar gas (BTO etching), HF solution (PEO etching), and ICP-RIE with CF<sub>4</sub>/O<sub>2</sub> gas (NOA61 removal). After LED chip isolation using the SU8 polymer, an Au electrode was deposited onto the p-ohmic contacts to fabricate flexible vertically structured  $\mu$ LEDs. The authors thank the Center for University-wide Research Facilities (CURF) at Jeonbuk National University for XRD (D8 ADVANCE, BRUKER).

### Electrical, optical, and mechanical measurements of flexible $\mu$ LEDs

Luminescence-current-voltage (L-I-V) characteristics of flexible  $\mu$ LEDs were measured simultaneously using a Keithley

4200-SCS and by AvaSpec-UIS2048-RS optic spectroscopy (Avantes Corp.). Mechanical fatigue tests were conducted using a periodic-bending-motion machine (customized equipment) and a Keithley 230 source meter.

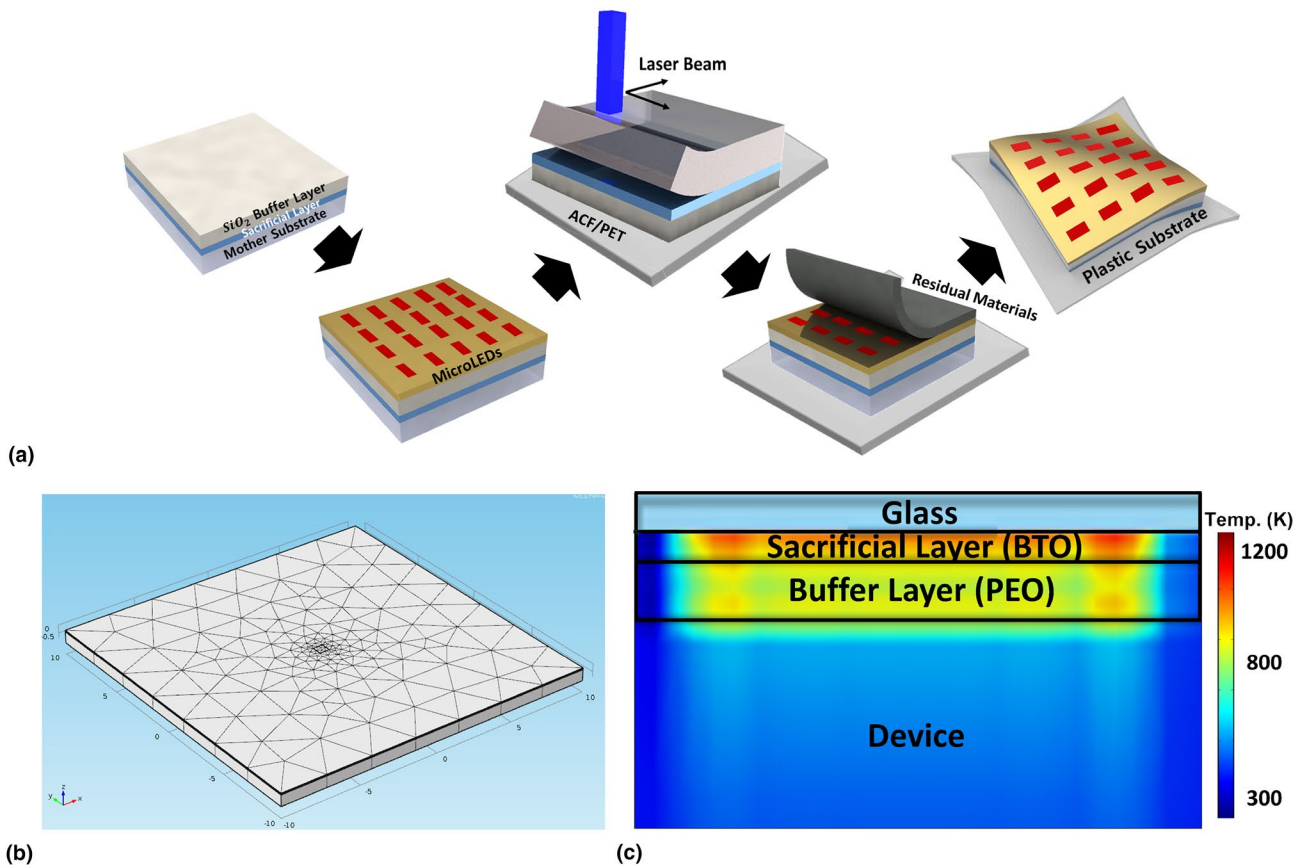
## Results and discussion

Figure 1(a) shows three-dimensional (3D) schematics of vertically structured flexible  $\mu$ LEDs using the ILLO-based thin-film transfer process. The specific processes are as follows. First, (i) a 300-nm-thick BTO film was grown on a transparent glass substrate as a sacrificial layer. Subsequently, a 1- $\mu$ m-thick PEO thin film was deposited onto the BTO as a mechanical/thermal buffer layer. (ii) The fabricated  $\mu$ LED arrays were attached to a PEO/BTO/glass carrier substrate using NOA 61. The carrier substrate is a temporary transfer medium that can securely maintain the freestanding device structure, irrespective of the external mechanical strain during the delamination procedure. (iii) After removing the GaAs wafer, the  $\mu$ LED arrays on the carrier wafer were bonded onto Au/PET film by ACF-based thermos-compressive process (annealing temperature: 160°C, pressure: 4 MPa, pressing time: 30 s). UV laser shots focused at the BTO-glass interface were irradiated through the transparent glass substrate. Because the interfacial adhesion of the BTO/glass was decreased due to the light-material interaction, the  $\mu$ LED arrays on the buffer layer were peeled off the carrier substrate. (iv) Residual materials of BTO, PEO, and NOA 61 were sequentially removed using SF<sub>6</sub>-based dry etching, HF wet etching, and CF<sub>4</sub>-based dry etching, respectively. (v) After fabricating the Au/Cr top electrodes, a passivation layer was coated on the top surface to protect the device from external stresses (see Fig. S1 in the Supporting Information for details of the fabrication procedure).

When laser shots with a high-energy density (>500 mJ cm<sup>-2</sup>) were applied to the light-reactive sacrificial material, the material temperature immediately rose to more than thousands of Kelvins. Because the laser-induced heat shock potentially affects the lower  $\mu$ LED device, the temperature distribution of the device was theoretically calculated by FEM simulation prior to the actual experiments [Fig. 1(b and c)]. Figure 1(b) displays a mesh refinement image of a  $\mu$ LED on the PEO/BTO/glass substrate, which was modeled identically using the actual dimensions of the device, such as thickness, width, and length. The laser-induced heat was simulated using Eq. (1).

$$Q + \nabla(k\nabla T) = \rho C \frac{\partial T}{\partial t}, \quad (1)$$

where  $Q$  is the laser-induced heat,  $k$  is the thermal conductivity,  $\rho$  is the material density,  $C$  is the specific heat (PEO, BTO, or glass), and  $T$  is the temperature of the device. According to the simulation results, the BTO-glass interfacial temperature instantly increased to ~1267 K upon exposure to laser at 750 mJ cm<sup>-2</sup>, as shown in Fig. 1(c). The 1- $\mu$ m-thick buffer PEO layer successfully dissipated the laser-induced heat to the



**Figure 1.** (a) Fabrication procedure of flexible  $\mu$ LEDs via the inorganic laser lift-off (b) Mesh refinement image of a  $\mu$ LED on  $\text{SiO}_2/\text{BTO}/\text{glass}$  substrate for FEM simulation (c) Temperature distribution obtained by FEM calculation when the BTO sacrificial layer was exposed to the laser of power density  $750 \text{ mJ cm}^{-2}$ .

outside, minimizing thermal shock to the lower device. In addition to the heat dissipation effect of the buffer layer, the device maintained its structure during the ILLO process because of the nanosecond pulsed laser beam.<sup>[24,25]</sup>

The attachment material between the  $\mu$ LED and the PEO/BTO/glass carrier substrate is especially important for the stable maintenance of the device structure during the ILLO process with extremely high thermal/mechanical stresses. To obtain the optimal adhesive, several materials, including the PDMS polymer, Pd–In alloy, SU8 photoresist, and optical adhesive, were investigated in the ILLO. Figure 2 shows the microscopic images of the laser-reacted material surfaces. After irradiating UV laser shots between the BTO layer and the glass, the lower device/PEO layers were exfoliated from the glass substrate. During the ILLO, two-dimensional laser beams of dimensions  $625 \mu\text{m} \times 625 \mu\text{m}$  were periodically scanned over the entire device area. The PDMS-attached sample displayed a few cracks in the laser-overlapped area [Fig. 2(a)], and the Pd–In metallic bonded sample had voids/defects [Fig. 2(b)], inducing mechanical damage to the devices. On the other hand, the exfoliated surfaces with the SU8 photoresist or optical adhesive were clean without any cracks or defects, as shown

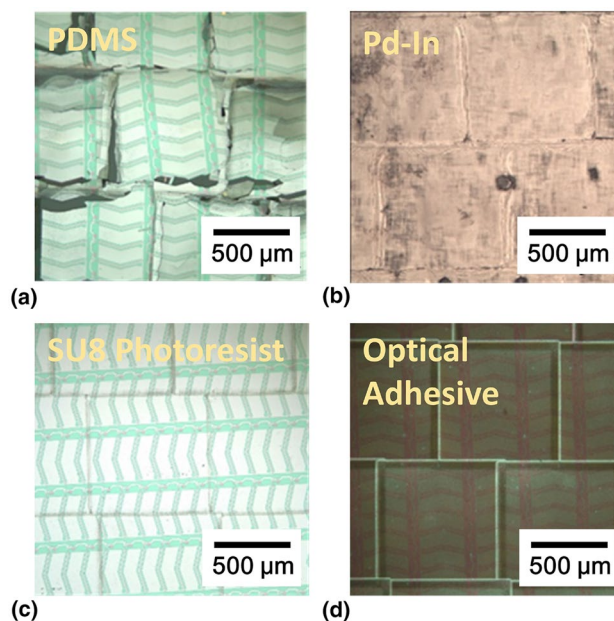


**Figure 2.** Microscopic images of the sample surface after the laser lift-off using (a) PDMS polymer, (b) Pd–In alloy, (c) SU8 photoresist, and (d) optical adhesive as attaching materials.

in Fig. 2(c and d). Despite the mechanical stability of the SU8 photoresist as the attaching material, the removal method of SU8 (piranha etching or acid-based wet thermal etching) was considerably harsh compared with that of the optical adhesive ( $\text{CF}_4/\text{O}_2$  gas-based dry etching), and the optical adhesive was optimally chosen as the attaching material for the ILLO.<sup>[26–28]</sup>

Thin-film transfer using the ILLO process was accomplished using a limited group of inorganic sacrificial materials, such as hydrogenated amorphous silicon (a-Si:H), lead zirconate titanate ( $\text{PbZr}_x\text{Ti}_{1-x}\text{O}_3$ ; PZT), and gallium nitride (GaN). The exfoliation mechanism of existing sacrificial materials using high-energy lasers is generally known as material decomposition.<sup>[29,30]</sup> However, because the phenomenon of BTO-assisted ILLO has not yet been investigated, we implemented material characterization of the laser-irradiated BTO surface after the lift-off process. Figure 3(a) shows the XRD curve of the as-deposited BTO thin film, indicating the typical form of an amorphous film. In contrast, the XRD curves in Fig. 3(b) show peak formation due to the laser–BTO interaction, indicating the increased crystallinity of BTO at various laser energy densities (550, 750, and 950  $\text{mJ cm}^{-2}$ ). To optimize the laser energy density, microscopic images of the BTO surface were obtained after ILLO. As shown in Fig. 3(c), when BTO was exposed to the 550  $\text{mJ cm}^{-2}$  laser, the material reaction was insufficient to peel off the glass substrate. The BTO layer was shattered by 950  $\text{mJ cm}^{-2}$  laser shots owing to their excessive power [Fig. 3(d)], while a laser power of 750  $\text{mJ cm}^{-2}$  was highly desirable for application to the ILLO because of the clear surface of the laser-irradiated material without any defects or cracks (magnified optical image shown in Fig. 3(e)). To precisely evaluate the BTO surface after the ILLO process, scanning electron microscopy (SEM) and atomic force microscopy (AFM) analyses were performed on the irradiated area with a laser power density of 750  $\text{mJ cm}^{-2}$ . As shown in the upper inset of Fig. 3(e), the laser-irradiated BTO surface had a randomly distributed nanostructure with an average roughness ( $R_a$ ) of 7.719 nm (Fig. S2). Nanostructures with widths of hundreds of micrometers are observed on the surface of the twice-laser-irradiated BTO, indicating an  $R_a$  of 11.993 nm (Fig. S3). Based on these results, the crystallized BTO nanostructures decreased the adhesion force between the device and the carrier substrate by reducing the contact area and enabled the film quality to be maintained after the ILLO process because of their superior flatness. Residues left on the surface after the ILLO process could be easily removed through the SF6-based dry etching process, bringing environmental advantages in the post-process compared to existing sacrificial materials of a-Si:H, PZT, and GaN.<sup>[17,18]</sup>

Finally, vertically structured flexible  $\mu\text{LEDs}$  were realized using a BTO-based ILLO to verify the practical usability of the developed process. Figure 4(a) shows a magnified optical microscopy image of the AlInGaP  $\mu\text{LED}$  array on a carrier substrate (NOA 61/PEO/BTO/glass) before the ILLO process. The  $\mu\text{LED}$  array was composed of chips of dimensions 80  $\mu\text{m} \times 80 \mu\text{m}$  chips with an interspace of 40  $\mu\text{m}$ . As shown in

the inset of Fig. 4(a) and Fig. S4, the  $\mu\text{LED}$  successfully emitted red light, showing peak emission wavelength of 653.5 nm and sharp peak with full-width at half maximum (FWHM) of 37.7 nm. Figure 4(b) shows a photograph of the flexible  $\mu\text{LED}$  under bending conditions. The  $\mu\text{LEDs}$  were selectively transferred onto 100- $\mu\text{m}$ -thick PET film, widening the interspace between the chips from 80 to 160  $\mu\text{m}$ . For realizing the selective  $\mu\text{LED}$  transfer, 50  $\mu\text{m} \times 55 \mu\text{m}$ -sized laser shots with 750  $\text{mJ cm}^{-2}$  were irradiated to the BTO layer, minimizing the laser-overlapped area without any cracks or breakdown of the devices. Because only the laser-reacted BTO area was peeled off the carrier substrate, the interspace between the  $\mu\text{LEDs}$  could be freely modulated by selective release onto the flexible substrate to achieve the desired purpose. The upper and lower insets of Fig. 4(b) show magnified microscopic and SEM images of the successfully fabricated flexible device, respectively. The SEM was analyzed in the Center for University-wide Research Facilities (CURF) at Jeonbuk National University. Optical and electrical properties of the flexible  $\mu\text{LED}$  were characterized by L–I–V curves, as shown in Fig. 4(c). As shown in the curves, the turn-on voltage ( $V_T$ ) increased 0.21 V, and irradiance of the  $\mu\text{LED}$  decreased 0.12  $\text{mW mm}^{-2}$  after the ILLO process. Furthermore, the property change of the device was negligible under the bent state with 1 cm bending radius, showing 0.12 V  $V_T$  and 0.14  $\text{mW mm}^{-2}$  degradation. Figure 4(d) shows the excellent mechanical reliability of the flexible  $\mu\text{LED}$  during the bending fatigue test. Although the mechanical test was implemented over 1000 periodic bending cycles with a bending radius of 1 cm, the irradiance of the device was only degraded by  $\sim 0.3 \text{ mW mm}^{-2}$ . In addition, the  $V_T$  of the  $\mu\text{LED}$  increased by approximately 4.29%, indicating the mechanical stability of the developed device. Based on these results, the BTO thin film has substantial potential as a sacrificial layer in the ILLO process for emerging flexible and wearable devices.

## Discussion

We developed a new ILLO technique for realizing vertically structured flexible  $\mu\text{LEDs}$  using a BTO sacrificial layer. To minimize thermal damage to electronic devices during the ILLO process, the light irradiation conditions were optimized to a power density of 750  $\text{mJ cm}^{-2}$  based on theoretical simulations and experimental analyses. Although the temperature of the BTO layer increased to  $\sim 1300$  K by laser irradiation, the lower devices were stably protected by the PEO-based thermal buffer layer. An optical adhesive was chosen as the carrier substrate for the ILLO, maintaining the structure of thin-film devices without any defects or cracks despite the harsh thermal/mechanical stresses in the film exfoliation process. The exfoliated surface after the ILLO was scrutinized via XRD, SEM, and AFM analyses for confirming the peeling-off stability of the BTO sacrificial layer at 750  $\text{mJ cm}^{-2}$  laser, showing superior flatness ( $R_a = 7.719$  nm). Finally, vertically structured flexible  $\mu\text{LEDs}$  were realized on

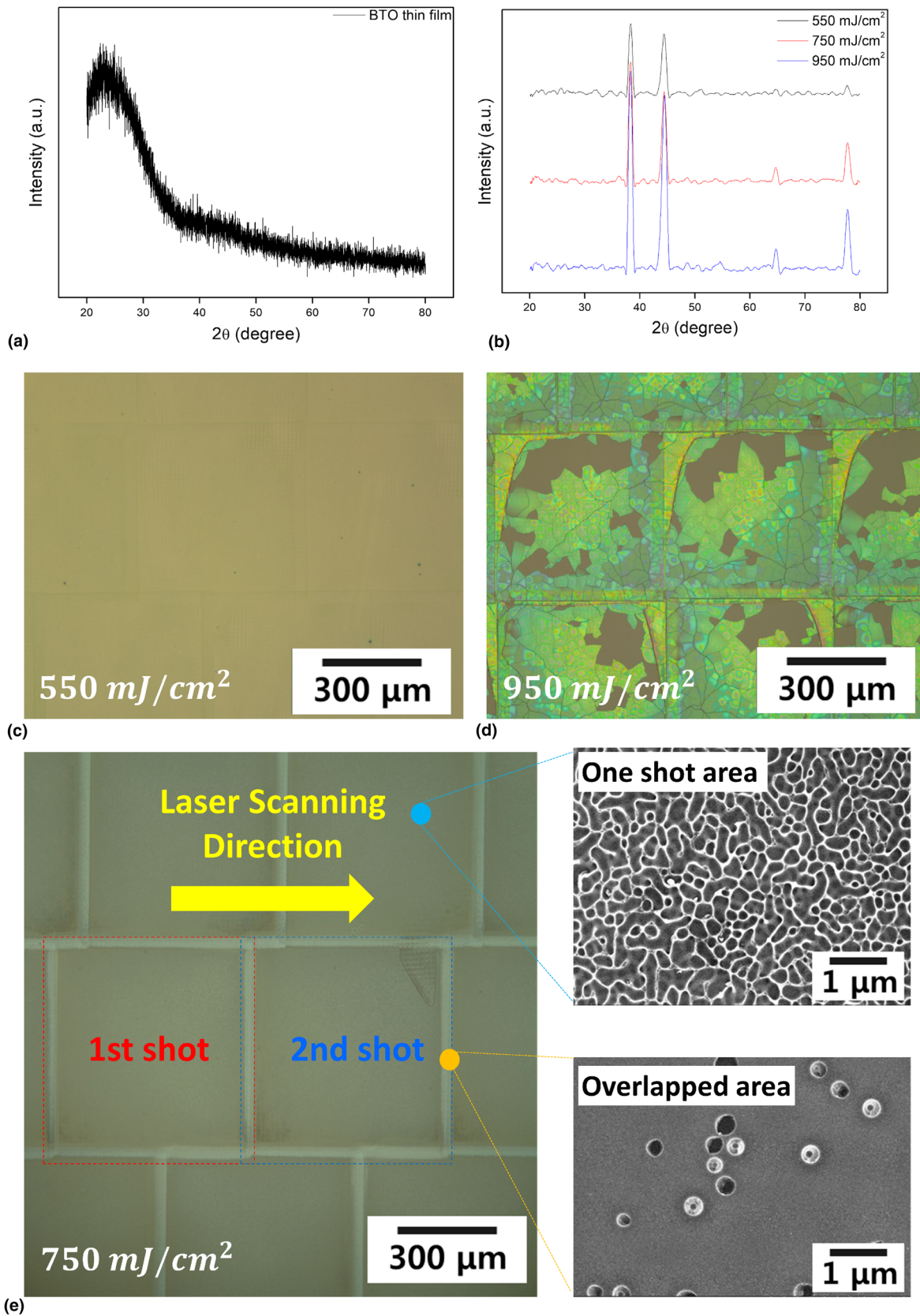


**Figure 3.** XRD curves of (a) as-deposited and (b) laser-reacted BTO thin films. Microscopic images of BTO thin films irradiated by lasers of power densities of (c)  $550 \text{ mJ cm}^{-2}$  and (d)  $950 \text{ mJ cm}^{-2}$ . (e) Magnified optical image and SEM results of  $750 \text{ mJ cm}^{-2}$  laser-irradiated BTO thin film after the inorganic laser lift-off.

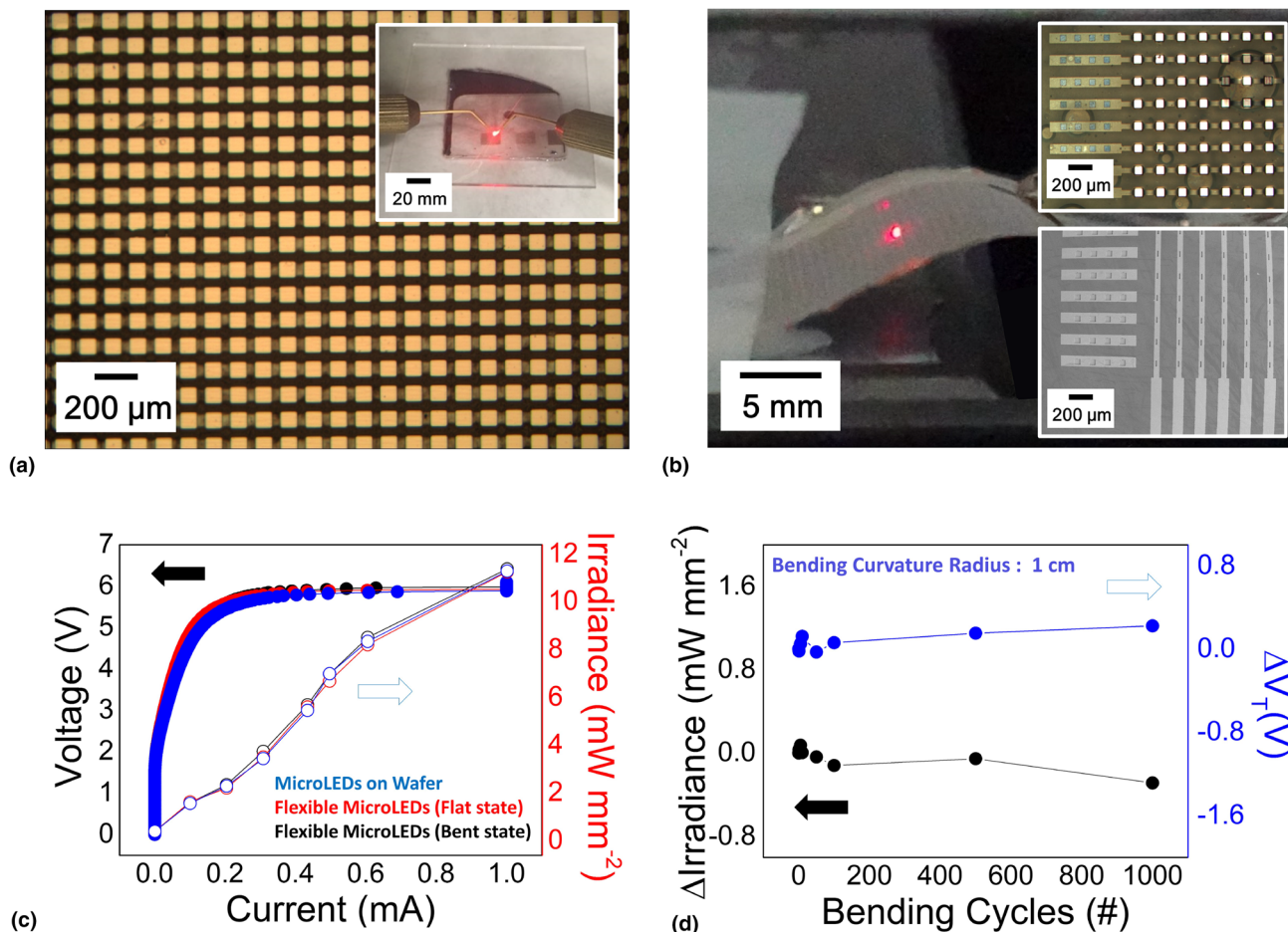


**Figure 4.** (a) Microscopic image of the AllnGaP  $\mu$ LED arrays attached onto BTO/SiO<sub>2</sub>/glass substrate. The inset image shows an illuminating  $\mu$ LED on the BTO/SiO<sub>2</sub>/glass substrate before the inorganic laser lift-off process. (b) Photograph of flexible red  $\mu$ LED on PET film under the bent state. The upper inset displays a magnified image of the selectively transferred  $\mu$ LED arrays. The lower inset presents a SEM image of the flexible  $\mu$ LED. (c) L-I-V curve of the red  $\mu$ LED on the rigid wafer (blue) and the flexible  $\mu$ LED under flat (red)/bent states (black) (d) Durability test results of the flexible red  $\mu$ LED (bending curvature radius: 1 cm).

a 100- $\mu$ m-thick PET film using BTO-assisted transfer and ACF packaging methods. The interspace of flexible  $\mu$ LEDs could be freely modulated by the selective transfer of the ILLO, satisfying the purpose of the final device. The optical and electrical properties of the flexible  $\mu$ LED were maintained with and without the thin-film device lift-off process. The mechanical robustness of the  $\mu$ LED was examined by bending durability tests of  $10^3$  periodic bending/unbending cycles, which showed a negligible  $V_T$  degradation of  $\sim 4.29\%$ . We believe that the developed BTO-based ILLO strategy provides an effective approach for achieving the emerging applications of high-performance flexible and wearable displays of various sizes, including digital signage, monitors, and smart devices.

## Acknowledgments

This work was supported by the National Research Foundation of Korea (NRF) grants funded by the Ministry of Science, ICT and Future Planning (MSIT) (NRF-2022R1F1A1066064, 2022R1A4A3033320, 2022R1A2C4002037 and 2022R1A4A3032923), and Nano·Material Technology Development Program through the NRF funded by MSIT (2009-0082580).

## Data Availability

All data in this study are available from the corresponding author on reasonable requests.

## Declarations

### Conflict of interest

The authors declare no conflict of interest.

### Supplementary Information

The online version contains supplementary material available at <https://doi.org/10.1557/s43579-023-00389-4>.

## References

- H. Lee, H.E. Lee, H.S. Wang, S. Kang, D. Lee, Y.H. Kim, J.H. Shin, Y. Lim, K.J. Lee, B. Bae, *Adv. Funct. Mater.* **30**, 2005610 (2020)
- H. Yeon, H. Lee, Y. Kim, D. Lee, Y. Lee, J.-S. Lee, J. Shin, C. Choi, J.-H. Kang, J.M. Suh, H. Kim, H.S. Kum, J. Lee, D. Kim, K. Ko, B.S. Ma, P. Lin, S. Han, S. Kim, S.-H. Bae, T.-S. Kim, M.-C. Park, Y.-C. Joo, E. Kim, J. Han, J. Kim, *Sci. Adv.* **7**, 1–11 (2021)
- Y. Jeong, H.E. Lee, A. Shin, D. Kim, K.J. Lee, D. Kim, *Adv. Mater.* **32**, 1907522 (2020)
- C. Choi, H. Kim, J.-H. Kang, M.-K. Song, H. Yeon, C.S. Chang, J.M. Suh, J. Shin, K. Lu, B.-I. Park, Y. Kim, H.E. Lee, D. Lee, J. Lee, I. Jang, S. Pang, K. Ryu, S.-H. Bae, Y. Nie, H.S. Kum, M.-C. Park, S. Lee, H.-J. Kim, H. Wu, P. Lin, J. Kim, *Nat. Electron.* **5**, 386–393 (2022)
- S.-M. Kang, H.E. Lee, H.S. Wang, J.H. Shin, W. Jo, Y. Lee, H. Lee, D. Lee, Y.H. Kim, T.-S. Kim, K.J. Lee, B.-S. Bae, *ACS Energy Lett.* **6**, 4097–4107 (2021)
- H. Song, J. Jang, M. Peddigari, S. Pattipaka, Y. Min, K.-I. Park, C.K. Jeong, H.E. Lee, J.H. Park, H.-Y. Lee, W.-H. Yoon, J. Ryu, G.-T. Hwang, *J. Mater. Chem. A* **11**, 3364–3372 (2023)
- J. Park, Y. Lim, S.Y. Cho, M. Byun, K. Park, H.E. Lee, S.D. Bu, K. Lee, Q. Wang, C.K. Jeong, *Small* **18**, 2104472 (2022)
- J.H. Shin, J.H. Park, J. Seo, T.H. Im, J.C. Kim, H.E. Lee, D.H. Kim, K.Y. Woo, H.Y. Jeong, Y. Cho, T. Kim, I. Kang, K.J. Lee, *Adv. Mater.* **33**, 2007186 (2021)
- M. Peddigari, J.H. Park, J.H. Han, C.K. Jeong, J. Jang, Y. Min, J.-W. Kim, C.-W. Ahn, J.-J. Choi, B.-D. Hahn, S.Y. Park, W.-H. Yoon, D.-S. Park, D.-Y. Jeong, J. Ryu, K.J. Lee, G.-T. Hwang, *ACS Energy Lett.* **6**, 1383–1391 (2021)
- H.E. Lee, J.H. Shin, J.H. Park, S.K. Hong, S.H. Park, S.H. Lee, J.H. Lee, I. Kang, K.J. Lee, *Adv. Funct. Mater.* **29**, 1808075 (2019)
- H.E. Lee, *Electronics* **10**, 2644 (2021)
- J. Shin, H. Kim, S. Sundaram, J. Jeong, B.-I. Park, C.S. Chang, J. Choi, T. Kim, M. Saravanapavanantham, K. Lu, S. Kim, J.M. Suh, K.S. Kim, M.-K. Song, Y. Liu, K. Qiao, J.H. Kim, Y. Kim, J.-H. Kang, J. Kim, D. Lee, J. Lee, J.S. Kim, H.E. Lee, H. Yeon, H.S. Kum, S.-H. Bae, V. Bulovic, K.J. Yu, K. Lee, K. Chung, Y.J. Hong, A. Ougazzaden, J. Kim, *Nature* **614**, 81–87 (2023)
- H.E. Lee, D. Lee, T.-I. Lee, J. Jang, J. Jang, Y.-W. Lim, J.H. Shin, S.-M. Kang, G.-M. Choi, D.J. Joe, J.H. Kim, S.H. Lee, S.H. Park, C.B. Park, T.-S. Kim, K.J. Lee, B.-S. Bae, *A.C.S. Appl. Mater. Interfaces.* **14**, 28258–28269 (2022)
- J.H. Lee, Y. Ahn, H.E. Lee, Y.N. Jang, A.Y. Park, S. Kim, Y.H. Jung, S.H. Sung, J.H. Shin, S.H. Lee, S.H. Park, K.S. Kim, M.S. Jang, B.J. Kim, S.H. Oh, K.J. Lee, *Adv. Healthc. Mater.* **12**, 2201796 (2023)
- H.E. Lee, J.H. Park, D. Jang, J.H. Shin, T.H. Im, J.H. Lee, S.K. Hong, H.S. Wang, M.S. Kwak, M. Peddigari, C.K. Jeong, Y. Min, C.H. Park, J.-J. Choi, J. Ryu, W.-H. Yoon, D. Kim, K.J. Lee, G.-T. Hwang, *Nano Energy* **75**, 104951 (2020)
- J.H. Shin, J.H. Park, J. Seo, T.H. Im, J.C. Kim, H.E. Lee, D.H. Kim, K.Y. Woo, H.Y. Jeong, Y. Cho, T. Kim, I. Kang, K.J. Lee, *Adv. Mater.* **33**, 2007186 (2021)
- C. Zhu, D. Guo, D. Ye, S. Jiang, Y. Huang, *A.C.S. Appl. Mater. Interfaces.* **12**, 37354–37362 (2020)
- N. Yulianto, G.T.M. Kadja, S. Bornemann, S. Gahlawat, N. Majid, K. Triyana, F.F. Abdi, H.S. Wasisto, A. Waag, *A.C.S. Appl. Electron. Mater.* **3**, 778–788 (2021)
- J. Bian, L. Zhou, B. Yang, Z. Yin, Y. Huang, *Appl. Surf. Sci.* **499**, 143910 (2020)
- S. Bornemann, N. Yulianto, H. Spende, Y. Herbani, J.D. Prades, H.S. Wasisto, A. Waag, *Adv. Eng. Mater.* **22**, 1901192 (2020)
- J. Bian, F. Chen, H. Ling, N. Sun, J. Hu, Y. Huang, *Int. J. Heat Mass Transf.* **188**, 122609 (2022)
- J. Seo, Y. Kim, W.Y. Park, J.Y. Son, C.K. Jeong, H. Kim, W.-H. Kim, *Appl. Surf. Sci.* **487**, 1356–1361 (2019)
- Y. Kim, J.M. Suh, J. Shin, Y. Liu, H. Yeon, K. Qiao, H.S. Kum, C. Kim, H.E. Lee, C. Choi, H. Kim, D. Lee, J. Lee, J.-H. Kang, B.-I. Park, S. Kang, J. Kim, S. Kim, J.A. Perozek, K. Wang, Y. Park, K. Kishen, L. Kong, T. Palacios, J. Park, M.-C. Park, H. Kim, Y.S. Lee, K. Lee, S.-H. Bae, W. Kong, J. Han, J. Kim, *Science* **377**, 859–864 (2022)
- M. Asadirad, Y. Gao, P. Dutta, S. Shervin, S. Sun, S. Ravipati, S.H. Kim, Y. Yao, K.H. Lee, A.P. Litvinchuk, V. Selvamaniakam, J.-H. Ryou, *Adv. Electron. Mater.* **2**, 1600041 (2016)
- C.K. Jeong, K.-I. Park, J.H. Son, G.-T. Hwang, S.H. Lee, D.Y. Park, H.E. Lee, H.K. Lee, M. Byun, K.J. Lee, *Energy Environ. Sci.* **7**, 4035–4043 (2014)
- A.R. Mackintosh, A.J.C. Kuehne, R.A. Pethrick, B. Guilhabert, E. Gu, C.L. Lee, M.D. Dawson, G. Heliotis, D.D.C. Bradley, *J. Phys. D: Appl. Phys.* **41**, 094007 (2008)
- M. Holmes, J. Keeley, K. Hurd, H. Schmidt, A. Hawkins, *J. Micromech. Microeng.* **20**, 115008 (2010)
- A. Mehboudi, J. Yeom, *J. Micromech. Microeng.* **28**, 035002 (2018)
- D.H. Jung, J.H. Park, H.E. Lee, J. Byun, T.H. Im, G.Y. Lee, J.Y. Seok, T. Yun, K.J. Lee, S.O. Kim, *Nano Energy* **61**, 236–244 (2019)
- T.H. Im, D.Y. Park, H.K. Lee, J.H. Park, C.K. Jeong, D.J. Joe, K.J. Lee, *Part. Part. Syst. Charact.* **34**, 1600429 (2017)

**Publisher's Note** Springer Nature remains neutral with regard to jurisdictional claims in published maps and institutional affiliations.

Springer Nature or its licensor (e.g. a society or other partner) holds exclusive rights to this article under a publishing agreement with the author(s) or other rightsholder(s); author self-archiving of the accepted manuscript version of this article is solely governed by the terms of such publishing agreement and applicable law.